A New Multi-Camera Approach For Lane Departure Warning

Amol Borkar, Monson Hayes, and Mark T. Smith

Georgia Institute of Technology, Atlanta, GA, USA {amol@gatech.edu}
Chung-Ang University, Seoul, Korea {mhh3@gatech.edu}
Kungliga Tekniska Högskolan, Stockholm, Sweden {msmith@kth.se}

Abstract. In this paper, we present a new multi camera approach to Lane Departure Warning (LDW). Upon acquisition, the captured images are transformed to a bird's-eye view using a modified perspective removal transformation. Then, camera calibration is used to accurately determine the position of the two cameras relative to a reference point. Lane detection is performed on the front and rear camera images which are combined using data fusion. Finally, the distance between the vehicle and adjacent lane boundaries is determined allowing to perform LDW. The proposed system was tested on real world driving videos and shows good results when compared to ground truth.

Keywords: Lane departure warning; multi camera calibration; data fusion; non-overlapping camera networks.

1 Introduction

Driver Assistance (DA) systems are common accessory in today's passenger and commercial vehicles. DA systems as the name suggests are systems that provide aid or feedback to the driver of a vehicle. One example of such a system is Lane Departure Warning (LDW). LDW is a safety feature that informs the driver if the vehicle appears to change lanes unless certain conditions are met e.g. turn indicator is on. The hardware often consists of a single camera which acquires images out of the front windshield that are analyzed to determine if the vehicle is within a certain distance of a lane boundary.

Although LDW has been in research for many years, it has only been recently that LDW systems have started appearing in luxury cars and as after market products. Variations of the Time to Lane Crossing (TLC) are some of the most popular techniques used for LDW [1–4]. Using a "look-ahead" approach, the future position of the vehicle is estimated based on the steering angle and by extrapolating detected lane positions, then the driver is warned if a lane crossing is predicted. The lane detection component of LDW often produces noisy results; consequently, the extrapolated estimates may not accurately represent future lane positions leading to false signaling. Other LDW techniques involve determining the angles or orientations of detected lane boundaries to hypothesize a distance metric [5–7]. Actual distance to the adjacent boundaries is not computed. In the proposed work, we compute the immediate distance between the vehicle and adjacent boundaries using known camera geometries. In addition, we add a second camera that looks out of the rear windshield. This provides redundant lane boundary position information which is used in data fusion.

Since we are combining data from multiple cameras, calibration is important. Calibration for stereo and n-camera setups is often performed using variations of standard test patterns like checkerboard to establish a baseline [8]. However, these techniques require each camera to be able to see the same checkerboard. Since our cameras are facing in opposite directions, the checkerboard methods are ineffective. Work on calibration for non-overlapping camera networks has been conducted in [9–11]. The method shown in [9, 10] uses a planar mirror while [11] uses a moving rig to calibrate each camera. However, the rig movement appears arbitrary which can severely affect the estimates of camera positions. A similar experiment with a multi camera setup for vehicular applications has been shown in [12]; however, the method used to merge information from the two cameras is only stated briefly and lacks details. Additionally, calibration of opposite facing cameras is not discussed. In our work, we have devised a new yet simple calibration technique that allows to accurately determine the position of the two cameras in the vehicle.

This paper is organized as follows: subsequent to the introduction, preprocessing in the form of a geometric transformation applied to acquired images is explained. Then, the details of camera calibration and data fusion are described. Finally, LDW is completed by explaining the technique used to measure the distance to lane boundaries. The proposed approach was compared to a single camera LDW system as well as ground truth and showed good results when tested on real world driving videos.

2 Pre-Processing

In a camera image, lane markings appear as lines that decrease in thickness and converge near the horizon. This can be seen on the left in Fig. 1. Consequently, feature extraction can become difficult since the line features change as a function of distance from the camera due to the effects of perspective. As a result, the camera acquired images first undergo a geometric transformation known as Inverse Perspective Mapping (IPM) to remove the effects of perspective from the image [13]. With IPM, the captured images are transformed to appear as a birds-eye view with lane markers now appearing as nearly parallel lines. In addition, the thickness of these lines remain constant in the IPM image as shown on the right in Fig. 1. The camera configuration is shown in Fig. 2. The mapping from world co-ordinates $(x, y, z = 0)$ to image co-ordinates (r, c) is given as

$$r(x) = \frac{M-1}{2}\left(1 + \frac{h - x' \cdot \tan\theta_o}{h \cdot \tan\theta_o + x'} \cdot \cot\alpha_v\right) + 1 \quad (1)$$

$$c(x, y) = \frac{N-1}{2}\left(1 - \frac{y'}{h \cdot \sin\theta_o + x' \cdot \cos\theta_o} \cdot \cot\alpha_u\right) + 1 \quad (2)$$

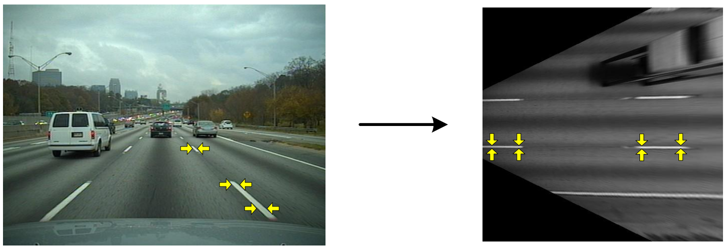

Fig. 1: Pre-processing stage.

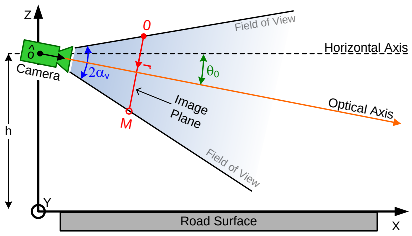

(a) Side view.

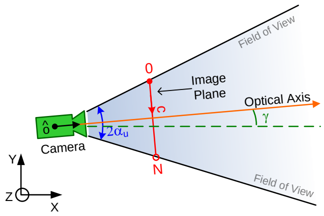

(b) Top view.

Fig. 2: Camera parameters.

where h is the height of the camera, θ_o is the pitch, α_u is the horizontal field of view, α_v is the vertical field of view, γ is the yaw, and $(M \times N)$ is the size of the camera image. Furthermore

$$\begin{bmatrix} x' \\ y' \end{bmatrix} = \begin{bmatrix} \cos\gamma & -\sin\gamma \\ \sin\gamma & \cos\gamma \end{bmatrix} \begin{bmatrix} x \\ y \end{bmatrix} \tag{3}$$

provides the yaw correction by rotating the world co-ordinates about the optical center of the camera. This mapping differs slightly from the technique described in [13] where the horizontal and vertical fields of view of the camera are assumed to be equal. However, in most commercial camera hardware, these values are different.

3 Camera Calibration

In camera calibration, an origin needs to be specified. This point is chosen as the center of the vehicle as shown in Fig. 3 and denoted as $\mathbf{P_o} = \begin{bmatrix} 0 & 0 & 0 \end{bmatrix}^T$. The positions of the front and rear cameras relative to $\mathbf{P_o}$ are then determined. These position are denoted as $\mathbf{P_f}$ for the front camera and $\mathbf{P_r}$ for the rear camera. $\mathbf{P_r}$ is also oriented looking out of the back of the vehicle which results in its IPM image being rotated 180°. Since small measurement errors in $\mathbf{P_f}$ and $\mathbf{P_r}$ could lead to critical errors during data fusion used later, the accuracy of these measurements is verified by comparing to reference data subject to certain constraints. The

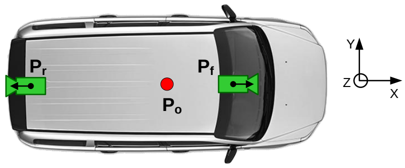

Fig. 3: Position of the origin and two cameras.

reference data is made up of images captured while driving at a constant speed near the middle of a straight road where the distance between adjacent lane boundaries is constant and uniform. Both cameras undergo basic calibration to determine yaw (γ) and pitch (θ_o) which prevents the lane boundaries from appearing skewed or tilted in the IPM image. Therefore, the cameras are now 180° opposed and facing in opposite directions along the X-axis of the reference co-ordinate system shown in Fig. 3. Sample front and rear camera images are shown in Fig. 4. Correctness is assumed in the measured X and Y co-ordinates

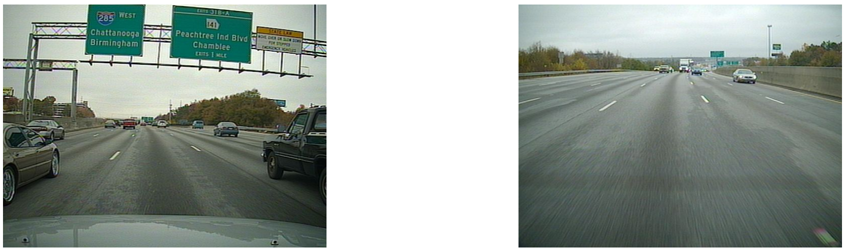

(a) Front camera image. (b) Rear camera image.

Fig. 4: Sample camera images.

of $\mathbf{P_f}$. The techniques described below accurately determine the height of $\mathbf{P_f}$ as well as the translation of $\mathbf{P_r}$ relative to $\mathbf{P_o}$.

3.1 Height measurement

We combine Eq. (1) and (2) to determine the mapping of a pixel from the camera to world co-ordinates as

$$Y(r,c) = h\left(\frac{[1-2(\frac{c-1}{N-1})]\tan\alpha_u}{\sin\theta_o - [1-2(\frac{r-1}{M-1})]\tan\alpha_v\cos\theta_o}\right) \tag{4}$$

We choose two points (r, c_1) and (r, c_2) on adjacent lane boundaries in the camera image and find their corresponding mappings to the IPM domain as $Y(r, c_1)$ and $Y(r, c_2)$ respectively as shown in Fig. 5. Since it not possible to park on the highway and physically measure the distance between adjacent lane boundaries,

(a) Two points in the camera image. (b) Two points in the IPM image.

Fig. 5: Mapping points from the camera image to IPM image.

we refer to Federal Highway Administrations (FHA) handbook regarding specification for painted markings [14] where it is stated that the distance between lane boundaries on highways is on average 12ft. Using this information, we can set

$$Y(r, c_1) - Y(r, c_2) = \mathit{\Delta} Y = 12 \text{ feet} \tag{5}$$

Hence, we substitute Eq. (4) in Eq. (5) and solve for h as

$$h = \mathit{\Delta} Y \left(\frac{\sin\theta_o - [1 - 2(\frac{r-1}{M-1})] \tan\alpha_v \cos\theta_o}{2[\frac{c_2 - c_1}{N-1}] \tan\alpha_u} \right) \tag{6}$$

Similarly, we can repeat this procedure to determine the height of the rear camera.

3.2 Offset between cameras

If the two cameras are not aligned properly, there will be a visible offset between the lane markings when observed in each IPM image. This is illustrated in Fig. 6 by placing the two IPM images side by side. Since the $\mathbf{P_f}$ is inline with the origin, the offset is adjusted by translating the rear camera IPM image along the Y-axis till the lane markings line up correctly. The translation in the IPM image is scaled to world units to determine the actual offset between the two cameras.

3.3 Distance between cameras

To determine the distance between the cameras, we need to find objects with corners in each IPM image. In our case, we use the diamond from the high occupancy vehicle (HOV) lane. This is shown in Fig. 7. Since the vehicle is commuting at a constant speed and knowing the time delay since the diamond from the front camera IPM image reappears in the rear camera IPM image, the total covered distance can be computed as

$$w = \text{Speed} \times \text{Time Delay} \tag{7}$$

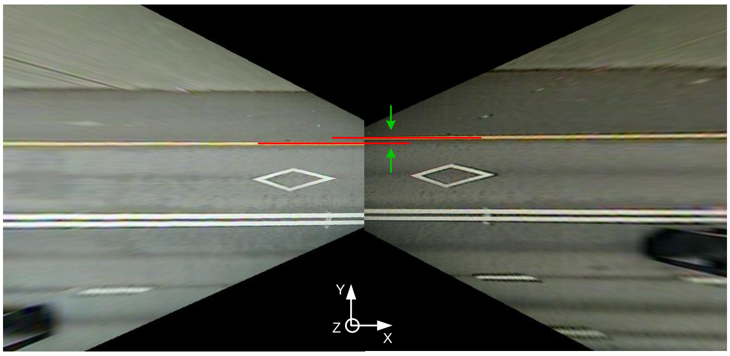

Fig. 6: Error in camera camera alignment. This results in lane markings being offset from one view to the other.

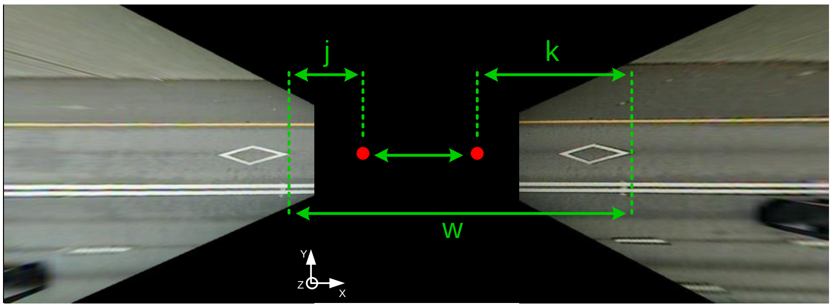

Fig. 7: Determining the distance between the cameras.

By setting $(x = 0, y = 0)$ in Eq. (3), the optical center of each camera relative to its IPM image can be determined and is illustrated by the red dots in Fig. 7. Since the lens used in this implementation has a focal length of 5mm, it is safe to assume that optical center is analogous to the camera position. As a result, it is possible to determine the distance j or k between a specific point on the diamond and the camera itself. Consequently, the distance between the cameras can estimated as

$$\text{Distance between cameras} = w - (j + k) \tag{8}$$

After completing the three verification steps described above, the position of the front camera is determined as $\mathbf{P_f} = \begin{bmatrix} 2.0 & 0.0 & 4.79 \end{bmatrix}^T$ and rear camera as $\mathbf{P_r} = \begin{bmatrix} -7.51 & -0.48 & 4.94 \end{bmatrix}^T$ relative to $\mathbf{P_o}$. The units are in feet.

4 Lane Detection

Lane detection is performed using the technique presented in [15] on both forward and rear camera views. Following IPM, the transformed image is converted from RGB to YCbCr to aid in color segmentation. Then, the images are cross-correlated with a collection of predefined templates to find candidate lane regions. These regions then undergo connected components analysis, morphological operations, and elliptical projections to approximate positions of the lane markers. The implementation of the Kalman filter enables tracking lane markers on curved roads while RANSAC helps improve estimates by eliminating outliers [15].

5 Data Fusion

In a standalone IPM image, the optical center e.g. $\mathbf{P_f}$ is at the origin. Each pixel in the IPM image has a certain (x, y) co-ordinate relative its optical center. This approach is acceptable when dealing with a single camera; however, when dealing with multiple cameras, a common co-ordinate system needs to be established.

In our implementation, $\mathbf{P_o}$ is chosen as the origin of this space and shown as a red dot in Fig. 8. The two green dots in Fig. 8 represent $\mathbf{P_f}$ and $\mathbf{P_r}$. Next, a transformation $\mathbf{T_f}$ that maps only the (x, y) co-ordinates of $\mathbf{P_o}$ to $\mathbf{P_f}$ is determined. This transformation when applied to the IPM image maps the (x, y) co-ordinates of each pixel to a location in the common co-ordinate system that is now relative to $\mathbf{P_o}$. Consequently, the lane boundaries detected in the front camera IPM image are also mapped to the common space and described by (x, y) co-ordinates relative to $\mathbf{P_o}$. A transformation mapping $\mathbf{P_o}$ to $\mathbf{P_r}$ is also computed and used to relocate the rear camera IPM pixels to the common co-ordinate space.

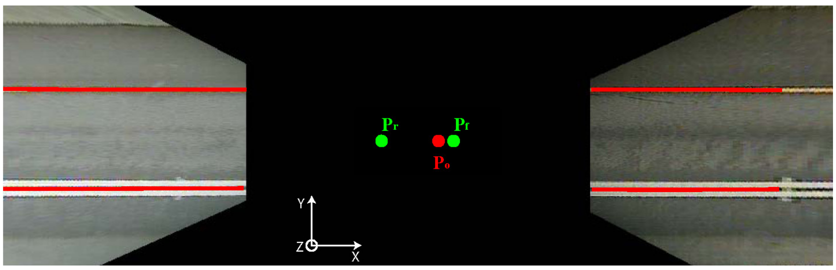

Fig. 8: Position of the origin and two cameras.

Upon completing the front and rear lane detections, data fusion in the form of a parametric linear spline connects the detected lane boundaries. Using an end point from each boundary as shown in Fig. 9, the locations of lane boundaries outside the cameras view can be estimated using Eq. (9).

$$\mathbf{Q}(\mathrm{t}) = \begin{bmatrix}(1\text{-t}) & \mathrm{t}\end{bmatrix} \begin{bmatrix}\mathbf{Q}_1 \\ \mathbf{Q}_2\end{bmatrix} \tag{9}$$

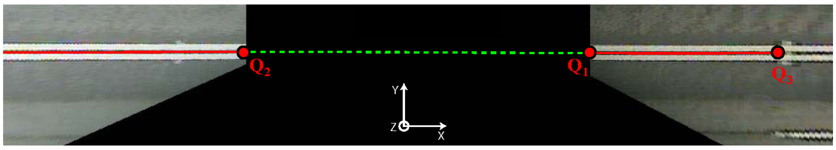

Fig. 9: Spline estimated boundary shown as dotted green line between the two end points $\mathbf{Q}_1$ and $\mathbf{Q}_2$.

6 Lane Departure Warning

Upon completing camera calibration and data fusion, the following is known:

1. Center of the vehicle.
2. Dimensions of a reference vehicle.
3. Location of lane boundaries.

Using the available information, the distance to the lane boundary (in feet) on either side of the vehicle can be calculated as:

$$\text{Distance to marking} = |\text{LB}_{x=0} - \text{sign}[\text{LB}_{x=0}](\frac{\text{Car\_Width}}{2})| \text{ feet} \qquad (10)$$

where $\text{LB}_{x=0}$ is simply the y-value of the estimated lane boundary from Eq. (9) evaluated at x=0. The orange bounding box in Fig. 10 depicts the dimensions of the reference vehicle in the common co-ordinate space with $\mathbf{P_o}$ as the red dot. Using Eq. (10), LDW can be systematically performed by warning the driver if the vehicle is within a minimum distance from a lane boundary.

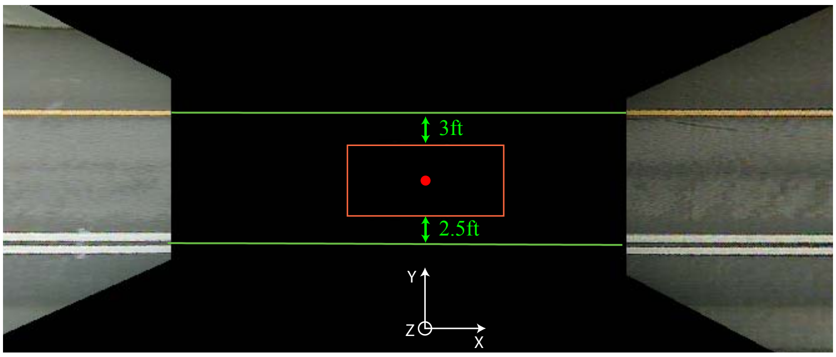

Fig. 10: Distance to lane boundaries on either side.

7 Results & Analysis

Two time-synchronized NTSC cameras were used in acquiring video streams for testing. The streams were captured while driving on roadways in and around Atlanta, GA, USA. Several minutes worth of videos were used in testing. The rear camera was inoperable at night without artificial illumination; hence, testing was restricted to day time only. Additionally, testing was conducted only on highway footage as most commercial LDW systems operate above 45mph [16, 17].

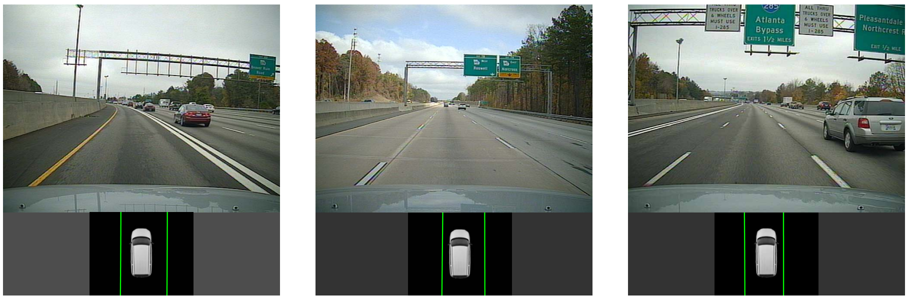

(a) (b) (c)

Fig. 11: Front camera image and estimated position of the vehicle within the lane.

In Fig. 11, a few examples of the images captured by the front camera with an overhead visualization estimating the position of the vehicle within a lane are shown. Fig. 12 shows an example of the vehicle approaching very close to a lane boundary over the duration of a clip. Fig. 12a - 12c shows the camera captured images with corresponding visualization. When the vehicle is within 0.75ft of a lane boundary, a warning is signaled. Hysteresis is used whereby the vehicle needs to travel more than 1ft away from the lane boundary for the warning to be disabled. This reduces flicker around the minimum distance threshold. Fig. 12d shows a plot of the estimated distance between the right lane boundary and vehicle over the duration of the video. The plot also shows a comparison between the multi camera approach, single camera approach and ground truth. To estimate distance using a single camera, we refer back to Fig. 9 and evaluate the line formed by $\mathbf{Q}_1$ and $\mathbf{Q}_3$ at x=0. A straight line model is less affected by noise in lane detection results; hence, it is used for extrapolation. Ground truth estimates are produced using cubic interpolation between the ground truth lane boundary locations in the front and rear camera images. In Fig. 12d, it can be observed that the estimates of the multi camera approach are often very close to the ground truth. The single camera approach fares well on straight roads but face difficult when encountered with a curve. Fig. 12e provides a visual comparison between the ground truth, single camera and multi camera approach when the vehicle encounters a turn in the test clip. The advantage of using the described multi camera setup is that estimating distances to the lane boundaries becomes an interpolation problem. With a single camera setup, it is an extrapolation problem which appears to be less accurate.

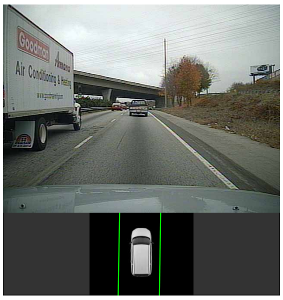

(a) Frame 73.

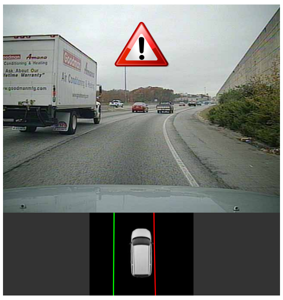

(b) Frame 289.

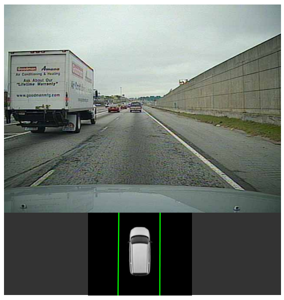

(c) Frame 429.

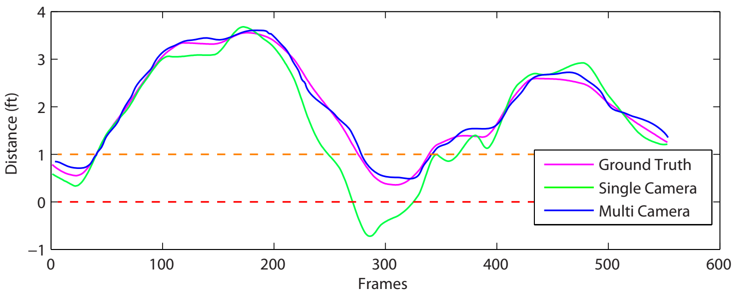

(d) Distance between vehicle and right lane marker.

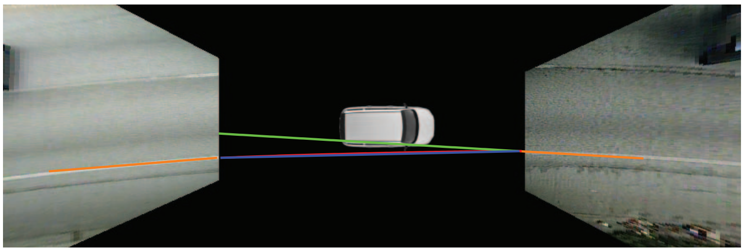

(e) Comparison between ground truth (red), single camera (green) and multi camera (blue) approach. Detected lane markings are shown in orange.

Fig. 12: An example of Lane Departure Warning (LDW).

Since the lane boundary estimates are calculated based on the findings of the front and rear lane detectors, errors in lane detection reflect directly on the lane boundary estimates. A few instances of incorrect lane detections shown in Fig. 13 resulted in incorrect estimates of the distances to the lane boundaries.

In addition, when an incomplete lane detection occurs i.e. only one boundary is detected in either front or rear camera images, the estimates around the vehicle cannot be determined. This is shown in Fig. 13c.

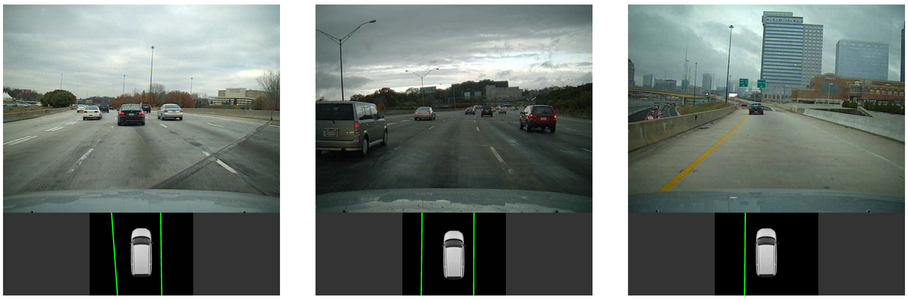

(a) (b) (c)

Fig. 13: A few examples where the multi-camera approach faces difficulty.

8 Conclusion

Presented in this paper is a novel approach to Lane Departure Warning (LDW) using multiple cameras. First, the captured images undergo an improved Inverse Perspective Mapping (IPM) transform to produce a bird's-eye view image. Then, camera calibration is used to accurately determine the position of two cameras. Following lane detection, data fusion is used to connect the detected lane boundaries from one camera view to the other. By determining the distance between the vehicle and lane boundaries, an LDW system is realized. The proposed setup showed good results when tested with real world driving videos. The multi camera approach also produced estimates close to the ground truth on both straight and curved roads in the test data while the single camera approach faced difficulty on the curved roads.

9 Future Work

The presented work is part of on going research. The use of smooth curves instead of straight line estimates for lane boundaries will be explored. Handling situations when an incomplete lane detection occur needs to be investigated. Kalman or particle filters will be used to track $LB_{x=0}$ on either side of the vehicle. Additional tests with complex scenarios will be conducted. Illumination hardware to enable night time multi camera usage will be purchased.

References

1. D. LeBlanc, G. Johnson, P. Venhovens, G. Gerber, R. DeSonia, R. Ervin, C. Lin, A. Ulsoy, and T. Pilutti, "CAPC: A road-departure prevention system," *Control Systems Magazine, IEEE*, vol. 16, no. 6, pp. 61–71, 1996.
2. W. Kwon, J. Lee, D. Shin, K. Roh, D. Kim, and S. Lee, "Experiments on decision making strategies for a lane departure warning system," in *Robotics and Automation, 1999. Proceedings. 1999 IEEE International Conference on*, vol. 4. IEEE, 1999, pp. 2596–2601.
3. S. Kim and S. Oh, "A driver adaptive lane departure warning system based on image processing and a fuzzy evolutionary technique," in *Intelligent Vehicles Symposium, 2003. Proceedings. IEEE.* IEEE, pp. 361–365.
4. X. Dai, A. Kummert, S. Park, and D. Neisius, "A warning algorithm for Lane Departure Warning system," in *Intelligent Vehicles Symposium, 2009 IEEE.* IEEE, pp. 431–435.
5. P. Hsiao, C. Yeh, S. Huang, and L. Fu, "A portable vision-based real-time lane departure warning system: day and night," *Vehicular Technology, IEEE Transactions on*, vol. 58, no. 4, pp. 2089–2094, 2009.
6. Q. Lin, Y. Han, and H. Hahn, "Real-time Lane Detection Based on Extended Edge-linking Algorithm," in *Computer Research and Development, 2010 Second International Conference on*, 2010, pp. 725–730.
7. Y.-C. Leng and C.-L. Chen, "Vision-based lane departure detection system in urban traffic scenes," in *Control Automation Robotics Vision (ICARCV), 2010 11th International Conference on*, 2010, pp. 1875–1880.
8. R. Hartley and A. Zisserman, *Multiple View Geometry in Computer Vision*, 2nd ed. Cambridge University Press, Apr. 2004.
9. P. Lébraly, C. Deymier, O. Ait-Aider, E. Royer, and M. Dhome, "Flexible extrinsic calibration of non-overlapping cameras using a planar mirror: Application to vision-based robotics," in *Intelligent Robots and Systems (IROS), 2010 IEEE/RSJ International Conference on.* IEEE, 2010, pp. 5640–5647.
10. R. Kumar, A. Ilie, J. Frahm, and M. Pollefeys, "Simple calibration of non-overlapping cameras with a mirror," in *Computer Vision and Pattern Recognition, 2008. CVPR 2008. IEEE Conference on.* IEEE, 2008.
11. F. Pagel, "Calibration of non-overlapping cameras in vehicles," in *Intelligent Vehicles Symposium (IV), 2010 IEEE.* IEEE, pp. 1178–1183.
12. S. Ieng, J. Vrignon, D. Gruyer, and D. Aubert, "A new multi-lanes detection using multi-camera for robust vehicle location," in *Intelligent Vehicles Symposium, 2005. Proceedings. IEEE.* IEEE, 2005, pp. 700–705.
13. M. Bertozzi and A. Broggi, "GOLD: a parallel real-time stereo vision system for generic obstacle and lane detection," *IEEE Transactions on Image Processing*, vol. 7, no. 1, pp. 62–81, 1998.
14. Federal Highway Administration, "Manual Uniform Traffic Control Devices," Nov. 2009. [Online]. Available: http://mutcd.fhwa.dot.gov/
15. A. Borkar, M. Hayes, and M. Smith, " A Template Matching And Ellipse Modeling Approach To Detecting Lane Markers," in *2010 Advanced Concepts for Intelligent Vision Systems (ACIVS 2010)*, 2010, pp. 179–190.
16. Infiniti USA, "2012 Infiniti M Specs & Options," 2011. [Online]. Available: http://www.infinitiusa.com/m/specs-options
17. Mercedes-Benz USA, "2011 Mercedes-Benz S550 Specs," 2011. [Online]. Available: http://www.mbusa.com/mercedes/vehicles/explore/specs/class-S/model-S550V